

# Kennard-Stepanov relation connecting absorption and emission spectra in an atomic gas

Peter Moroshkin,\* Lars Weller, Anne Saß, Jan Klaers, and Martin Weitz  
*Institute for Applied Physics, University of Bonn, Wegelerstr. 8, 53115 Bonn, Germany*  
 (Dated: December 2, 2024)

The Kennard-Stepanov relation describes a thermodynamic, Boltzmann-type scaling between the absorption and emission spectral profiles of an absorber, which applies in many liquid state dye solutions as well as in semiconductor systems. Here we examine absorption and emission spectra of rubidium atoms in dense argon buffer gas environment. We demonstrate that the Kennard-Stepanov relation between absorption and emission spectra is well fulfilled in the collisionally broadened atomic gas system. Our experimental findings are supported by a simple theoretical model.

PACS numbers: 05.20.-y, 32.70.Jz, 34.90.+q

Atomic spectroscopy in the gas phase is an area where electronic resonances can be investigated extremely well shielded from the external environment, in which case under linear spectroscopy conditions the absorption spectral profile of a line matches the emission spectral profile. This is in striking contrast to many observations of solid or liquid phase optical spectroscopy, where the coupling to phonons and other excitations causes a large variety of optical phenomena [1]. In some cases, as described by Kennard and Stepanov [2, 3], the coupling to the environment causes a simple and universal thermodynamic relation between the absorption and emission lineshapes. The so-called Kennard-Stepanov law states that the spectral profiles of absorption and emission  $\alpha(\omega)$  and  $f(\omega)$  respectively are related by  $f(\omega)/\alpha(\omega) \propto \exp(-\frac{\hbar\omega}{k_B T})$ , where  $T$  denotes the temperature of the sample. This Boltzmann-type scaling is known to be well fulfilled for many dye molecules in liquid solution [4] as well as for some semiconductor systems [5]. The Kennard-Stepanov relation is important for spectroscopic studies and offers prospects for non-contact temperature determinations. It also plays an important role in recent experiments on the thermalization of a photon gas by repeated absorption and emission processes and Bose-Einstein condensation of photons in a dye microcavity [6]. Indirectly, the Kennard-Stepanov relation enables the operation of alkali-vapor lasers in buffer gas broadened systems [7, 8].

We have studied the rubidium  $D$ -lines absorption and emission spectra at high pressure argon buffer gas conditions. The typical pressure broadened linewidth reaches a few nanometers, and approaches the thermal energy in frequency units  $k_B T/\hbar$ . We demonstrate that the ratio between observed absorption and emission spectral profiles well follows the frequency dependent scaling predicted by the Kennard-Stepanov law. Our experimental results are described by a theoretical model that is based on a thermal equilibrium between external atomic degrees of freedom and the internal structure of alkali-noble gas quasimolecules in the electronic ground and excited state submanifolds respectively. In general, the agreement between thermodynamic theory and experi-

ment improves for larger buffer gas pressures, which is attributed to be a signature for the role of three-body collisions for the thermalization.

Before proceeding, we note that it is known that the collisions between electronically excited state alkali atoms and noble gas perturbers are surprisingly elastic, so that a large number of collisions can occur without quenching of the excited state [9]. The interaction of atoms and light near the line centers is usually well described within the impact limit of the binary collisional model, which assumes short phase-changing collisions and the atom-light interaction mainly occurring at times where the atoms have unperturbed eigenfrequencies. In the impact limit the predicted lineshapes are symmetric, and the Kennard-Stepanov relation does not apply. For increased pressures, as the coupling by the light field experienced during the collision contributes significantly to the observed spectrum, the impact limit ceases to be fulfilled. A general description of absorption and emission probabilities requires a knowledge of the quasimolecular potential curves of the collision partners, a regime also known as collisionally aided excitation [10]. It furthermore has been noted that frequent atomic collisions can under suitable conditions lead to a thermalization of quasimolecular states [11, 12].

The Kennard-Stepanov relation can be straightforwardly derived [13] for a system with an electronic ground state  $|g\rangle$  and an electronically excited state  $|e\rangle$ , each of which are subject to an additional sublevel structure. We assume that the excited state lifetime is sufficiently long that its sublevel population (as well as the ground state manifold) acquires thermal equilibrium. The following derivation follows the treatment of Sawicki and Knox for rovibrational submanifolds in dye molecules [4]. Our aim is to generalize it to the here discussed problem of a collisionally broadened atomic system. The ratio between emission and absorption coefficient at a particular frequency  $\omega$  is

$$\frac{f(\omega)}{\alpha(\omega)} \propto \frac{\int g'(E')A(E',\omega)W_e(E')dE'}{\int g(E)B(E,\omega)W_g(E)dE}, \quad (1)$$

where  $E$  and  $E'$  are the energies in the electronic ground and excited state manifolds respectively and  $g(E)$  and  $g'(E')$  are the corresponding densities of states. Further,  $B(E, \omega)$  and  $A(E', \omega)$  denote the Einstein coefficients for absorption and spontaneous emission respectively. Note that the integrals in Eq. (1) must be carried out over both the bound and the free eigenstates, and include quasimolecular states as well as *e.g.* the atomic fine structure. In thermal equilibrium, the probabilities of occupation of sublevels are given by the Boltzmann factors  $W_g(E) = (1/Q_g) \exp(-E/k_B T)$  and  $W_e(E') = (1/Q_e) \exp(-E'/k_B T)$  in the lower and upper electronic states respectively, where  $Q_g$  and  $Q_e$  are the corresponding partition functions. The Einstein  $A-B$  relation here takes the form

$$g'(E')A(E', \omega)dE' = \frac{2\hbar\omega^3}{\pi c^2} g(E)B(E, \omega)dE. \quad (2)$$

Substituting this equation and the occupation probabilities  $W_g(E)$ ,  $W_e(E')$  into eq. (1) and using  $\hbar\omega_0 + E' = \hbar\omega + E$ , where  $\omega_0$  denotes the unperturbed atomic resonance frequency, yields the Kennard-Stepanov relation

$$\frac{f(\omega)}{\alpha(\omega)} \propto \exp\left[-\frac{\hbar(\omega - \omega_0)}{k_B T}\right], \quad (3)$$

which also can be written in the form

$$\ln\left[\frac{\alpha(\omega)}{f(\omega)}\right] = \frac{\hbar\omega}{k_B T} + C, \quad (4)$$

with  $C$  being a constant. We note that the same result as above can also be obtained in a model more closely following standard collisional theory [10], if we assume that the atomic motion is sufficiently slow so that the quasistatic approximation applies. The presence of a buffer gas atom at a distance  $r$  from the absorbing (radiating) atom causes a shift of the resonance frequency  $\omega - \omega_0 = (U_e(r) - U_g(r))/\hbar = \Delta U(r)$ , where  $U_g(r)$  and  $U_e(r)$  are the electronic ground and excited state potential curves respectively (assumed for simplicity to be isotropic). We now can rewrite Eq. (1) as

$$\frac{f(\omega)}{\alpha(\omega)} = \frac{\rho_e(r)4\pi r^2 g_e A(r, \omega) \left(\frac{d\Delta U}{dr}\right)^{-1}}{\rho_g(r)4\pi r^2 g_g B(r, \omega) \left(\frac{d\Delta U}{dr}\right)^{-1}}, \quad (5)$$

where  $\rho_g(r)$  and  $\rho_e(r)$  are the probabilities to find a buffer gas atom at a distance  $r$  relatively to the absorber (emitter) atom in the ground and excited state respectively. In thermal equilibrium we have

$$\rho_{g,e}(r) = \rho_0 \exp\left[-\frac{U_{g,e}(r)}{k_B T}\right], \quad (6)$$

with  $\rho_0$  chosen such that the buffer gas atomic distribution is normalized. In Eq. (5), we have not reduced the factor  $(d\Delta U/dr)^{-1}$ , which arises from the dependence

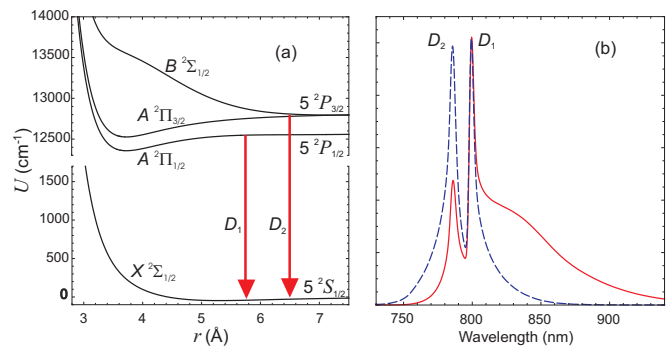


FIG. 1. (color online) (a) Theoretical rubidium-argon interaction potentials [14], as relevant for collisional broadening of the rubidium  $D$ -lines. (b) Calculated fluorescence (solid red line) and absorption (dashed blue line) spectra of rubidium atoms perturbed by collisions with argon buffer gas atoms.  $T = 400$  K,  $p = 180$  bar.

of the transition frequency on the interatomic distance. In the limit of the validity of the quasistatic approach, *i.e.* for  $d\Delta U/dr$  differing from zero, one can again verify the Kennard-Stepanov relation when combining this equation with a corresponding expression for Eq. (2).

Fig. 1(a) gives calculated quasistatic rubidium-argon molecular potential curves, as derived by ab-initio methods in Ref.[14]. For large interatomic distance, the shown curves asymptotically approach the energy of rubidium atoms in the  $5S_{1/2}$ ,  $5P_{1/2}$ , and  $5P_{3/2}$  electronic states. The interaction potential slope  $d\Delta U/dr$  approaches zero both at large interatomic separations as well as at minima within the potential curve. The corresponding points usually give rise to sharp peaks in the absorption and emission spectra, which are well known not to be adequately described by quasistatic lineshape theory. Using such potential curves, we have for a more complete characterization of our system calculated both absorption and emission lineshapes of the rubidium  $D$ -lines in the high pressure argon buffer gas regime, following standard methods of a unified line broadening theory [10, 15, 16], see also the Supplemental Information. Typical calculated results for the rubidium  $D$ -lines absorption and emission spectra are shown in Fig. 1(b) for a buffer gas pressure of 180 bar.

For an experimental determination of rubidium absorption and emission in dense buffer gas environment, we use a stainless steel pressure cell ( $\approx 2$  cm<sup>3</sup> inner volume) with sapphire windows to provide optical access. The cell is filled with rubidium metal and heated to temperatures in the range of 400 - 600 K, which provides a vapor-pressure limited rubidium density in the range of  $3 \times 10^{13}$  -  $5 \times 10^{16}$  cm<sup>-3</sup>. We use argon buffer gas pressures in the range of 20 - 200 bar, corresponding to a typical densities of order  $10^{21}$  cm<sup>-3</sup>. Rubidium atoms are excited with a beam from a Ti:sapphire laser, which can be tuned in a broad range around the rubidium  $D_1$  and

$D_2$  lines (with line centers at 795 nm and 780 nm respectively). The typical used beam power is 0.5 - 1.0 W on a 3 mm beam diameter. We collect the laser-induced fluorescence emitted in perpendicular direction to the excitation laser beam and analyze the fluorescence spectrally with a grating spectrometer of 1 nm resolution.

To allow for the investigation of atomic samples with low optical density, absorption spectra have been obtained by recording the total detected fluorescence power versus incident laser frequency, which gives a signal that is proportional to the absorption coefficient. In this way the rubidium density (and correspondingly the optical density) could be kept low enough to suppress reabsorption in the sample. This technique assumes that the quantum efficiency is near unity (or at least independent from wavelength), as is well established from [17]. By determining the fluorescence yield at different optical beam powers, we have in additional measurements verified that the laser intensity is low enough to avoid saturation.

In initial measurements, by recording fluorescence spectra at different incident laser wavelengths, we have verified that the spectral profile of the emitted fluorescence within experimental uncertainties is, at least in the high pressure buffer gas regime, largely independent on the wavelength of the excitation beam. This conclusion agrees with results obtained in earlier experiments of our group in the context of collision redistribution laser cooling of such dense rubidium-argon gas mixtures [17, 18]. The observed redistribution of fluorescence is attributed to the frequent collisions of rubidium atoms with argon atoms in the dense gas system.

Fig. 2(a) shows typical absorption (dashed blue line) and fluorescence (solid red line) spectra recorded at a temperature of 420 K and the buffer gas pressure of 180 bar. The profile in both cases shows two relatively sharp peaks, the line cores, near the positions of the rubidium  $D_1$  and  $D_2$  lines respectively on top of a very broad spectral wing, spanning nearly the complete shown spectral range of 730 - 940 nm. Noticeably, the line asymmetry of the absorption and emission spectra is quite opposite, with the absorption (emission) spectra having a more pronounced short (long) wavelength wing respectively. One may argue that the spectra thus roughly fulfill the mirror symmetry known *e.g.* from dye molecules in liquid solution [19]. Further, the relative peak heights differ in the two spectra. This is consistent with the predictions for a coupling of the alkali-noble gas quasimolecular states to the thermal environment in the dense gas ensemble. Fig. 2(b) shows the logarithm of the ratio of the corresponding absorption and the emission spectral profiles versus the optical wavenumber (which is directly proportional to frequency). In this representation, the Kennard-Stepanov relation predicts a linear dependence, see Eq. 4, which when plotted versus wavenumber has a slope of  $hc/k_B T$ . The dots in Fig. 2(b) are the corresponding experimental data of Fig. 2(a), and the solid

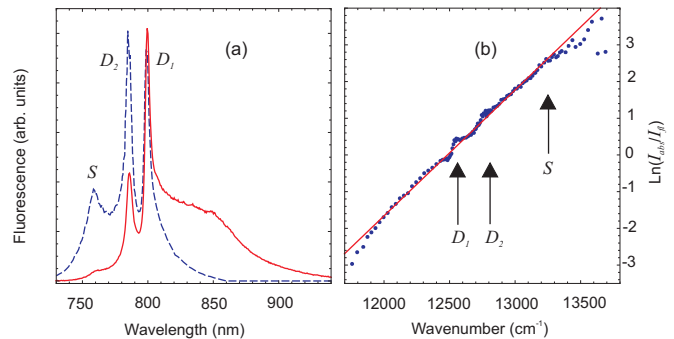


FIG. 2. (color online) (a) Experimental fluorescence (solid red line) and absorption (dashed blue line) spectra of the rubidium  $D$ -lines, in the presence of argon buffer gas;  $p = 180$  bar,  $T = 420$  K. (b) Corresponding Kennard-Stepanov plot, showing the logarithm of the ratio of the observed absorption and the emission spectral profile versus the optical wavenumber. The dots are the experimental data and the solid line is a guide for the eye with a slope  $hc/k_B T$ . The vertical arrows indicate the positions of the  $D_1$  and  $D_2$  transitions and of the blue satellite respectively.

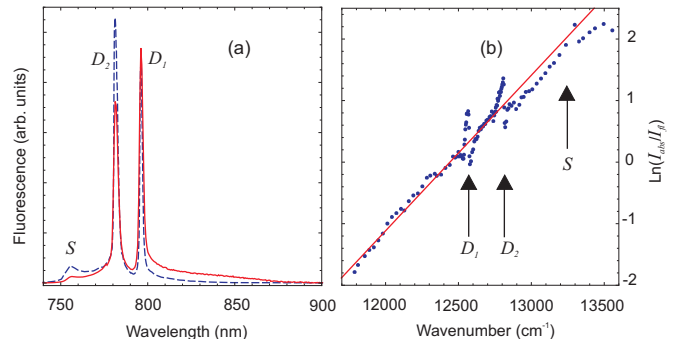


FIG. 3. (color online) Same as Fig. 3, but for  $p = 70$  bar buffer gas pressure and  $T = 570$  K. (a) Experimental fluorescence (solid red line) and absorption (dashed blue line) spectra of rubidium-argon gas mixture; (b) the corresponding Kennard-Stepanov plot.

red line has a slope of  $hc/k_B T$ , with  $T$  corresponding to the cell temperature. The good linearity of the experimental data, see the agreement with the red line, suggests that the Kennard-Stepanov law is well fulfilled in the observed spectral range. This is especially amazing when taking into account the complex individual lineshapes of the absorption and emission spectra, in a regime far from the impact limit. Remaining deviations from the linear dependence are seen in the vicinity of the  $D$ -lines resonance frequencies and at extreme red and blue detunings. The latter is attributed to technical limitations since in those spectral ranges the absorption (fluorescence) signal is already very low.

Fig. 3(a) shows absorption and emission spectra at somewhat lower buffer gas density, with  $T = 570$  K and  $p = 70$  bar. The cores of both rubidium  $D$ -lines have a smaller linewidth, and moreover the spectral wings are

less pronounced. Fig. 3(b) gives the logarithm of the ratio of the corresponding absorption and the emission profiles, which again shows a linear scaling that is in a good agreement with a slope relating to the cell temperature, as predicted by the Kennard-Stepanov law. We point out that the linewidths of the  $D$ -line cores in Fig. 3(a) are only a factor 2-3 larger than the spectral resolution of our spectrometer, so that the observed lineshape of the emission spectrum will thus already have instrumental contributions. Correspondingly, the visible spectrally sharp substructure near the  $D$ -lines resonances in Fig. 3(b) is still consistent with being purely instrumental. On the other hand, the deviations from the linear dependence at this lower buffer gas pressure are also larger far from resonance than in the case of the 180 bar pressure data. This shows the importance of a large collisional rate for the thermalization. In other measurements, we have observed rough agreement with the Kennard-Stepanov scaling down to argon buffer gas pressures of 40 bar.

The improved agreement of the ratio of absorption and emission with the Kennard-Stepanov law for larger pressures is attributed to the role of three-body collisions in the course of thermalization. This is understood in terms of a redistribution within (quasi-)bound states of the excited electronic manifold (see the potential minima of the  $A^2\Pi_{3/2}$  or  $A^2\Pi_{1/2}$  states in Fig. 1(a)) requiring one additional collisional partner beyond the argon-rubidium pair. Further, note that the thermalization within the excited state manifold also requires a redistribution between the rubidium fine structure components. In earlier work, the role of three-body collisions for fine structure changing collisions has been pointed out [12], which becomes increasingly important for the much larger buffer gas pressures used in the present work.

A detailed inspection of the data of Fig. 3(b), recorded at 70 bar buffer gas pressure shows that the data at higher wavenumbers beyond the  $D_2$  line has the same slope than the data recorded at lower frequencies, but a different offset. Contributions from the  $D_2$  ( $D_1$ ) line dominate for the high (low) frequency spectral data, and correspondingly the observed change in offset could be explained by assuming incomplete redistribution among the rubidium fine structure levels for the 70 bar data. In contrast, the 180 bar data of Fig. 2(b) well follows a single straight line, both at the positions of the blue and the red wings. We thus expect that at this higher pressure the relative population of  $5P_{1/2}$  and  $5P_{3/2}$  states is well distributed following Boltzmann's law. The redistribution results in an enhanced population of the energetically lower  $5P_{1/2}$  state, and a corresponding decrease of the  $D_2$ -line emission, see Fig. 3(a).

We next briefly discuss the agreement of the individual absorption and emission spectra with our calculated line shape spectra, as were shown in Fig. 1(b). We point out that the spectral widths of the line cores and their

pressure shifts have been investigated in some detail in early absorption spectroscopy studies [20]. Our experimental data for the individual absorption and emission spectra, see Figs. 2(a) and 3(a), exhibit qualitative agreement with the predictions, as shown in Fig. 1(b), with the largest deviation probably being the blue satellite, which is seen in the experimental data (labeled as ( $S$ )) but not visible in the theory spectrum. The calculations reproduce the observed bimodal character of the lines, consisting of relatively sharp line cores on top of a broad wing, as well as the experimental buffer gas pressure shift and line broadening for the  $D$ -lines transitions. An increase of the buffer gas density leads to a pronounced increase of the height of the wing with respect to the line core. This is understood from the increased probability of argon atoms being in the potential minima of the excited quasimolecular states at larger buffer gas pressure. In general, while lineshape calculations are a nontrivial task in the high pressure buffer gas regime, conclusions from statistical theory (including the Kennard-Stepanov relation) here apply with increasing accuracy.

To conclude, we have demonstrated that the Kennard-Stepanov relation, a thermodynamic frequency dependent scaling between absorption and emission spectra, is well fulfilled in observed rubidium  $D$ -lines spectra at high argon buffer gas pressures. In general, the agreement improves at larger buffer gas pressures, which is attributed to the role of three-body processes in both the thermalization of alkali-noble gas quasimolecular states and fine-structure changing collisions.

We expect that these findings add to the development of alkali-lasers [7, 8] as well as to studies of collisional redistribution laser cooling of dense gases [17, 18]. For non-contact temperature determinations in dense gases by means of the Kennard-Stepanov relation, auxiliary optical transitions with low oscillator strengths, as the blue  $5S - 6P$  transition in the rubidium atomic system, can be investigated to avoid reabsorption effects. A different perspective includes the thermalization of photon gases in dense pressure broadened gas samples within an optical microcavity. This may enable the operation of photon condensates in the vacuum ultraviolet regime when using optical transitions in noble gas atoms, as the  $5p^6(^1S_0) - 5p^5(^2P_{3/2})6s$  transition near 149 nm from the ground state to the lowest excited state of the xenon atom for photon thermalization.

## SUPPLEMENTAL INFORMATION

For calculations of absorption and emission lineshapes of rubidium atoms at high argon perturber densities a unified line broadening theory is used. The applied technique is also known as Anderson-Talman-theory [10]. In brief, absorption and emission spectra are obtained by a Fourier transform of an autocorrelation function of the

oscillating atomic dipole,  $\Phi(s)$ :

$$\Phi(s) = \left\langle \exp \left[ -\frac{i}{\hbar} \sum_{k=1}^N \int_t^{t+s} \Delta U(\mathbf{r}_k(t')) dt' \right] \right\rangle_t. \quad (7)$$

Here, it is assumed that the rubidium atom interacts with  $N$  argon atoms (perturbers) occupying positions  $\mathbf{r}_k$  and the angular brackets denote averaging over initial collision geometries. It is also assumed that the perturbers do not interact with each other and their motion is uncorrelated. Eq. 7 is simplified by neglecting the motion of individual perturbers and introducing the  $\mathbf{r}$ -dependent perturber density defined by eq. 6 of the main text, which gives

$$\Phi(s) \simeq \exp \left[ -\int \left( 1 - \exp \left[ -\frac{i}{\hbar} \Delta U(\mathbf{r})s \right] \right) \rho_{g(e)}(\mathbf{r}) d\mathbf{r} \right]. \quad (8)$$

The lineshapes presented in this paper, as shown in Fig. 1(a), were computed by using the theoretical *ab initio* Rb-Ar interaction potentials from [14]. Note that  $\Delta U(\mathbf{r})$  and  $\rho(\mathbf{r})$  are spherically symmetric in the case of the  $5^2S_{1/2}$  and  $5^2P_{1/2}$  states of Rb ( $X^2\Sigma_{1/2}$  and  $A^2\Pi_{1/2}$  potential curves) and are anisotropic for the  $5^2P_{3/2}$  state of Rb, for which  $A^2\Pi_{3/2}$  and  $B^2\Sigma_{1/2}$  potential curves describe Rb-Ar interaction along two orthogonal directions. Electronically-excited Rb atoms may form a bound state (quasimolecule) with an Ar atom located in a potential well of the state  $A^2\Pi_{3/2}$  or  $A^2\Pi_{1/2}$ . A contribution of those bound states is approximated as in [11] by allowing  $U_e(r)$  in eq. 6 to take negative values in the region of the potential well. A more detailed account of our calculations will be given elsewhere. Typical calculated fluorescence and absorption spectra are shown in Fig. 1(b). The largest disagreement of experimental lineshapes with calculations is at around 750 nm wavelength, where the experimental data show a blue satellite that in the calculated spectra is, depending on the buffer gas pressure, either weaker than in the experimental spectra or, as in Fig. 1(b), not seen at all.

Our calculations suggest that at even higher buffer gas densities than used in the present experiment the probability that an argon atom remains at very low distance to a rubidium atom in the electronically excited state manifold approaches unity. This then leads to a dominating contribution of a red satellite centered at 850 nm wavelength and a almost complete disappearance of the sharp  $D$ -lines spectral peaks.

The experimental absorption spectra have been determined by measuring fluorescence signals versus the incident laser wavelength, which allows us to use low optical density samples (see main text). To suppress a background from scattered incident laser beam radiation, a signal that is proportional to the absorption was obtained

by integrating the fluorescence yield from spectral regions offset from the excitation laser wavelength. The accuracy of this measurement is limited by the degree of spectral redistribution. We have verified that the obtained absorption profile at Ar pressures above 40 bar does in good accuracy not depend on the choice of the spectral region in which the fluorescence yield was integrated (complete redistribution). Our technique also assumes that the quantum efficiency is near unity, or at least is independent on the wavelength, as is well established experimentally for the alkali atom-noble gas mixture [17].

We thank H. Berriche for providing numerical data of rubidium-argon interaction potentials [14]. Financial support from the DFG (We 1785/15) and the ERC (IN-PEC) is acknowledged.

---

\* present address: RIKEN, Center for Emerging Matter Science, 2-1 Hirosawa, Wako, Saitama 351-0198, Japan; petr.moroshkin@riken.jp

- [1] See, e.g.: C. Klingshirn, *Semiconductor optics* (Springer, 2012).
- [2] E. H. Kennard, *Phys. Rev.* **11**, 29 (1918).
- [3] B. I. Stepanov, *Doklady Akad. Nauk SSSR* **112**, 839 (1957), *Soviet Phys. - Doklady*, **2**, 81 (1957).
- [4] D. A. Sawicki and R. S. Knox, *Phys. Rev. A* **54**, 4837 (1996).
- [5] Y. B. Band and D. F. Heller, *Phys. Rev. A* **38**, 1885 (1988).
- [6] J. Klaers, J. Schmitt, F. Vewinger, and M. Weitz, *Nature* **468**, 545 (2010).
- [7] R. V. Markov, A. I. Plekhanov, and A. M. Shalagin, *Phys. Rev. Lett.* **88**, 213601 (2002).
- [8] W. F. Krupke, *Prog. Quant. Electron.* **36**, 4 (2012).
- [9] E. Speller, B. Staudenmayer, and V. Kempster, *Z. Phys. A* **291**, 311 (1979).
- [10] N. Allard and J. Kielkopf, *Rev. Mod. Phys.* **54**, 1103 (1982).
- [11] R. E. M. Hedges, D. L. Drummond, and A. Gallagher, *Phys. Rev. A* **6**, 1519 (1972).
- [12] J. F. Sell, M. A. Gearba, B. M. Patterson, D. Byrne, G. Jemo, T. C. Lilly, R. Meeter, and R. J. Knize, *J. Phys. B* **45**, 055202 (2012).
- [13] D. E. McCumber, *Phys. Rev.* **136**, A954 (1964).
- [14] J. Dhiflaoui, H. Berriche, M. Herbane, A. G. AlSehimi, and M. C. Heaven, *J. Phys. Chem. A* **116**, 10589 (2012).
- [15] A. Royer, *Phys. Rev. A* **22**, 1625 (1980).
- [16] P. Moroshkin, V. Lebedev, and A. Weis, *Phys. Rev. A* **87**, 022513 (2013).
- [17] U. Vogl and M. Weitz, *Nature* **461**, 70 (2009).
- [18] U. Vogl, A. Saß, S. Haßelmann, and M. Weitz, *J. Mod. Optics* **58**, 1300 (2011).
- [19] J. R. Lakowicz, *Principles of fluorescence spectroscopy* (Kluwer Academic, New York, 1999).
- [20] S. Y. Ch'en and M. Takeo, *Rev. Mod. Phys.* **29**, 20 (1957).